THE JOURNAL OF PHYSICAL CHEMISTRY B

ARTICLE

pubs.acs.org/JPCB

Role of Conformation in $\pi-\pi$ Interactions and Polymer/Fullerene Miscibility

Katie Campbell,[†] Bilge Gurun,[†] Bobby G. Sumpter,[‡] Yonathan S. Thio,[†] and David G. Bucknall*[,†]

[†]School of Materials Science and Engineering, Georgia Institute of Technology, Atlanta, Georgia 30332, United States

[‡]Center for Nanophase Materials Sciences and Computer Science & Mathematics Division, Oak Ridge National Laboratory, Oak Ridge, Tennessee 37831, United States

ABSTRACT: The origin of the miscibility between C_{60} fullerene and a series of phenyl vinyl polymers has been investigated using a combination of wide-angle X-ray (WAXS) and neutron (WANS) scattering and density functional theory (DFT) computational modeling. The solubility limit of the C_{60} in the polymers was found to increase nonlinearly with increasing phenyl rings in the side groups from 1 wt % in polystyrene (PS) to 12 wt % in poly(9-vinylphenanthrene) (P9VPh). The DFT calculations showed that the polymer interacts with the fullerene preferentially via the phenyl groups in these vinyl polymers. However, due to the backbone these phenyl groups are unable to form the energetically favorable T-junction or planar $\pi-\pi$ stacks with the fullerene and are randomly oriented to the cage. The nonlinear increase in solubility is believed to be associated with shape conformity of the three-ring phenanthrene to the curvature of the fullerene.

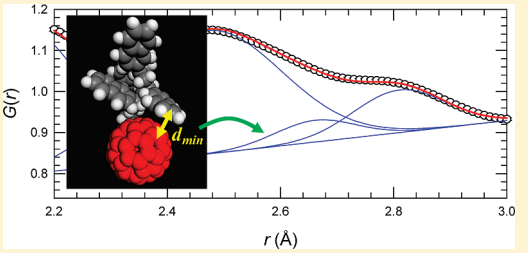

INTRODUCTION

Since their discovery fullerenes have been widely studied and consequently employed in numerous technological areas, including well publicized use in current state-of-the-art organic photovoltaic devices (OPVs). The solubility[1−12] and aggregation behavior,[13−26] as well as charge-transfer (CT) complex formation[27−32] of fullerenes, particularly C_{60}, in solution have been studied extensively. Despite these publications, it is arguable that the fundamental nature of molecular interactions with fullerenes is not that well understood. This is especially true in the case of polymer−fullerene interactions, and despite a few pieces of indirect data in the literature, for the most part the thermodynamics of polymer−fullerene interactions are even less well understood than small molecule interactions. Both theory[1,3,8,11,12] and experiment[2,4−6,9,10] agree that C_{60}−small molecule interactions are enhanced by increasing aromaticity which promotes $\pi-\pi$ interactions and by atoms much larger than carbon such as chlorine. Noncovalent interactions such as CT complex formation have been shown to improve solubility and dispersion with both fullerenes[33] and carbon nanotubes.[34−38]

Electron donating capability has also been shown to be important in improving fullerene interactions by allowing for complex formation between C_{60} and both small molecules[27−32] and polymers[33,39−41] as C_{60} is a willing electron acceptor. The strength of CT complexes formed between C_{60} and a variety of small molecules including the homologous series of benzene,[30] naphthalene, and phenanthrene[31] have been determined using the Benesi−Hildebrand theory and the association constant for complex formation.[42] In studies conducted by Yamaguchi and coworkers for short, cyclic polymer complexes with fullerenes, cyclic polymer complexes with C_{60} were shown to be several orders of magnitude stronger than those seen with small molecules.[41] These molecules are of particular relevance to the current studies because they are equivalent to the monomers of the polymers studied.

Laiho et al. also conducted investigations on C_{60} inclusion in poly(styrene-*b*-4-vinylpyridine) diblock copolymers where C_{60} was found to complex with the poly(4-vinylpyridine) block in solution upon aging. This complex formation was further shown to influence the microphase separation morphology of the block copolymer due to the energetic cost of incorporating the fullerenes into the system,[33] and further research with block copolymer−fullerene systems has shown that the dispersion of fullerenes can also greatly affect the degree of alignment that can be achieved in the microphase.[43]

Methods for improving the solubility and dispersion of fullerenes, particularly with polymers, have also been employed including modification of the fullerene cage with grafted polymer chains as the C_{60} cage is willing to accept up to six electrons.[44−46] Bonding just two polystyrene (PS) chains to the fullerene was shown to drastically improve the miscibility of C_{60} in a PS matrix, and PS-modified fullerenes were shown to disperse either as single molecules or small aggregates depending on the chain length of the polymer and the blend composition.[45] Fullerenes with up to six PS "arms" have also been successfully included in PS-based block copolymer systems, and the addition of PS arms to the C_{60} cage has been shown to force the fullerenes into the PS block.[44,46]

However, only limited investigation has been conducted regarding polymer−fullerene systems and further research is required to fully characterize the nature and forces responsible

Received: April 5, 2011
Revised: June 20, 2011
Published: June 22, 2011

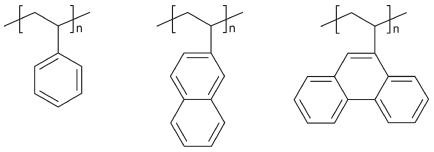

Figure 1. Polymer structures investigated experimentally with C_{60} for effects of increased aromaticity on dispersion: (a) polystyrene; (b) poly(2-vinylnaphthalene); (c) poly(9-vinylphenanthrene).

for these interactions. Understanding polymer/fullerene behavior is useful for a wide range of potential applications including nanoparticle templating and photovoltaic applications. While results of small molecule−C_{60} studies have some implications regarding polymer−C_{60} systems, the size of polymer structures and placement of interacting functional groups is likely to influence the magnitude of the interaction.

We have undertaken the systematic study of the effects of increased aromaticity in the side group of vinyl polymers on our ability to disperse fullerenes in amorphous polymer matrices of polystyrene, poly(2-vinylnaphthalene), and poly(9-vinylphenanthrene) using wide-angle X-ray scattering (WAXS). Also, we have examined the effects of molecular weight on the dispersion limit using three different molecular weights of polystyrene. We previously reported a miscibility limit of 0.5 wt % C_{60} with polystyrene of M_n = 100 kg/mol using a similar method.[43] Density functional theory (DFT) simulations have been used to better understand the nature of polymer−fullerene interactions and explain the dramatic improvement in miscibility seen with increasing $\pi-\pi$ interaction capability of vinyl polymers.

MATERIALS AND METHODS

Materials. HPLC grade toluene and ACS grade methanol were purchased from VWR International as solvent and nonsolvent respectively for polymer/fullerene blend preparation. C_{60} fullerene (purity 99.5+%) was used as received from VWR International. Polystyrene (PS) with M_n of 100 000 g/mol, PDI = 1.1, was used as a base system for investigation of aromaticity effects on C_{60} dispersion limits. Poly(2-vinylnaphthalene) (P2VN, M_n = 45 000 g/mol, PDI = 1.6) and poly(9-vinylphenanthrene) (P9VPh, M_n = 6800 g/mol, PDI = 1.13) were purchased from Polymer Source, Inc. Polymer structures are shown below in Figure 1. Two additional PS molecular weights (M_n = 41 400 g/mol, PDI = 1.02; M_n = 6240 g/mol, PDI = 1.04) were investigated for molecular weight effects. Both PS systems were purchased from Polymer Standards Service-USA, Inc. The molecular weights selected in this instance were directly comparable to those of the P2VN and P9VPh. Deuterated PS (dPS, M_n = 115 kg/mol, PDI = 1.04) was used for the wide angle neutron scattering measurements and were prepared in the same as for the hydrogenated analogues. All polymer materials were used as received.

Polymer/Fullerene Blend Preparation. Polymer and C_{60} were dissolved separately in toluene and sonicated for 30 min. The C_{60} solutions were then added to those of the polymer to give various compositions. The polymer−fullerene solutions were then sonicated for an additional 30 min before precipitation into cold, stirred methanol. The solid precipitates were then vacuum filtered and dried by annealing for 24 h at 125 °C in vacuum prior to scattering measurements. Pure polymers were treated in the same way for comparison to polymer−fullerene blends.

Wide Angle X-ray and Neutron Scattering Setup and Measurement. Wide angle X-ray scattering (WAXS) was conducted using a Rigaku Micro Max 002 X-ray generator operating a Cu Kα source at 45 kV and 0.66 mA and a R-axis VI++ detector. Polymer−fullerene blends were pressed into films using elevated temperature, and scattering from these samples was collected for 5 min. Data were corrected for film thickness prior to processing. Brittleness of some samples prevented film formation, particularly in the case of higher loadings C_{60} in P9VPh. In these cases powder samples were measured using glass capillary tubes with 1 mm diameter and wall thicknesses of 0.01 mm were used as purchased from Hamilton Research. Scattering was collected for 1 h for powder samples, and scattering from empty capillaries and air was collected for equal time to correct for background. AreaMax software was used for background subtraction and integration. It is important to note that both film and capillary measurements were conducted for pure PS, and no difference was observed in the WAXS patterns or dispersion limit.

Wide angle neutron scattering (WANS) measurements were made on the SANDALS beamline at the ISIS Neutron Facility (Rutherford Appleton Lab). The solid powders were measured in flat-plate 1 mm ZrTi alloy cells, which have a zero mean coherent scattering length and therefore do not contribute to the scattering. The normalized differential scattering cross-section as a function of scattering vector, q ($Å^{-1}$), was obtained after reducing and normalizing the data to absolute intensity using vanadium standards and correcting for the background, multiple scattering, and absorption. The real-space radial distribution functions, $G(r)$, were determined by Fourier transforming the differential scattering cross sections.

Density Functional Theory (DFT) Calculations. All-electron DFT calculations of C_{60} interacting with oligomers of the monomer structures shown in Figure 1 (5 monomer units of each type: styrene, 2-vinylnaphthylene, and 9-vinylphenanthrene) were performed using NWChem[47] with the local density (LDA) and generalized gradient approximation (GGA). The atom centered, contracted Gaussian basis set, 6-31G*,[48] was used during the calculation of self-consistent solution. The initial geometries for the different C_{60}−polymer systems were obtained by optimizing the geometry via energy minimization of the C_{60}−oligomers using Materials Studio 5.0 (Accelrys). The minimization was achieved using an algorithm that uses a cascade of steepest descent, conjugate gradient (Fletcher−Reeves algorithm) and Newton (BFGS algorithm) methods. To ensure a local energy minimum structure has not been found, a *NVT* molecular dynamics simulation was run on the lowest energy structures using a Nosé−Hoover thermostat at 298 K. The resulting structures from the MD simulation were subsequently run through the energy minimization protocol again and the resulting minimum energy structures used as the initial input for the DFT calculations. While this approach may not necessarily have obtained global energy minima for the structures, which in any case is achieved using the DFT calculations, it does significantly reduce the time taken for these calculations to converge.

It is now well-known that ab initio methods often can exhibit significant errors for nonbonded interactions unless very large basis sets are used in conjunction with highly correlated methods such as coupled-cluster with perturbative triple excitations, CCSD(T).[49,50] While most popular density functional approximations fail to describe London dispersion interactions, a large

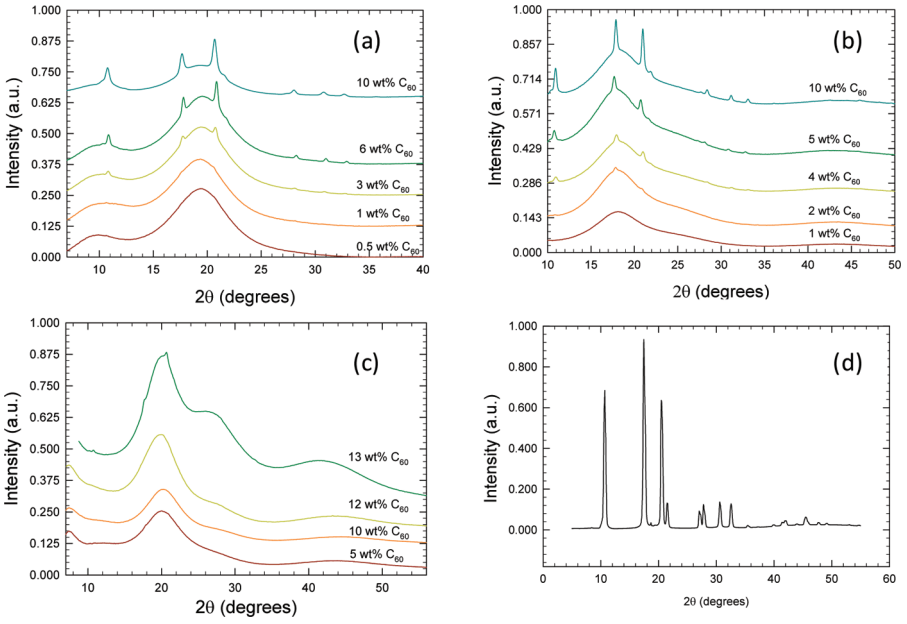

Figure 2. 1D WAXS patterns of blends of (a) PS_{100}, (b) P2VN, and (c) P9VPh with C_{60} and (d) pure C_{60}. The miscibility limit for each polymer system is determined by the appearance of fullerene crystalline peaks as seen at 1, 2, and 12 wt % for PS, P2VN, and P9VPh respectively. The data in figures (a)−(c) have been translated vertically for clarity.

number of studies have sought to improve theoretical methods for nonbonded interactions. For DFT, the simplest method conceptually is to add a damped, empirical dispersion term, yielding a method usually designated as DFT-D. This approach is simple and cost-effective and has demonstrated good results for nonbonded interactions in a variety of geometries.[51]

In this study, we have also used the DFT-D approach,[51] specifically the B97-D method as described by Vazquez-Mayagoitia et al.[49] to validate the relative strength and trends of the intermolecular interactions as computed from DFT-LDA. The gas phase monomer−C_{60} interaction energies are computed by $E_B = E_{mf} - E_{BSSE} - E_{def}$, where E_{mf} is the energy of the optimized polymer−fullerene pair and E_{BSSE} is used to eliminate the basis set superposition error (BSSE) by the counterpoise procedure as defined by $E_{BSSE} = \Sigma_i E_i(g)$, where $E_i(g)$ is the energy of monomer I at the geometry in the dimer with dimer basis functions present. The energy is also corrected for the deformation energy $E_{def} = \Sigma_i[E_i(opt) - E_i]$, where $E_i(opt)$ is the energy of the optimized species (fullerene or oligomer) and E_i is the energy of that species in its original geometry within the optimized total system. Finally, the relative amount of charge transfer that occurs at the nanoscale interface was estimated from the difference between a simple Mulliken population analysis of the C_{60}−oligomer and that for C_{60} and the oligomers. This is a very crude estimation of the charge transfer, but our goal was not to provide quantitative information but to attempt to capture relative trends.[52,53] A more quantitative approach would be to compute the explicit charge transfer integrals.[54]

RESULTS AND DISCUSSION

To determine the effect of increased aromaticity on the solubility of C_{60}, a homologous series of vinyl polymers (PS, P2VN, and P9VPh) have been investigated experimentally using WAXS measurements. All the polymers are fully amorphous, as shown by their WAXS patterns (Figures 2a−c). By comparison, aggregates of C_{60} are highly crystalline with a characteristic WAXS pattern of pure fullerene, as shown in Figure 2d. The observation of these characteristic Bragg peaks in the WAXS patterns as a function of increasing concentration of C_{60} was used to define the upper limit of solubility of the fullerene in that particular polymer. This method is insensitive to the initial onset of clustering of the C_{60} molecules from initially fully dispersed fullerenes to the point where two or more C_{60} molecules cluster together. Determination of the aggregation number at the experimentally derived solubility limit was attempted using AFM measurements but is below the resolution limit of the instrument. Assuming the aggregates are near the polymer matrix surface, we estimate that the resolution limit for detecting fullerene aggregates using AFM is around 5 nm in diameter. Using this figure as an upper limit, this would mean aggregates are forming that contain up to O(100) C_{60} atoms. The 1D WAXS patterns for each series of the three polymer blends with varying C_{60} content are shown in Figure 2. At zero or very low concentrations of C_{60} in each polymer, the WAXS patterns from the polymers shows typical amorphous scattering. At higher loadings of C_{60} above the solubility limit, the three strongest peaks in the WAXS pattern of pure C_{60} (Figure 2d) are clearly evident at 2θ = 10.8, 17.8, and 20.9°.

In all of the 1D WAXS patterns, the sharp crystalline diffraction peaks are due to C_{60} fullerene aggregation, while the broad amorphous peaks are due to the polymers. On the basis of the presence of these peaks in the WAXS patterns, we have previously shown a miscibility limit between 0.5 and 1.0 wt % C_{60} in PS (M_n = 100 kg/mol) using WAXS as shown in Figure 2a.[43] The upper limit of 1.0 wt % is indicated by the observation of weak C_{60} diffraction peaks in the WAXS data. The dispersion limit increases to 1−2 wt % C_{60} in the case of C_{60}/P2VN blends and to 12−13 wt % for P9VPh blends.

The increase in the miscibility with increasing aromaticity can be anticipated on the basis of published solvent−fullerene solubility data. However, the magnitude of the increase between

dx.doi.org/10.1021/jp203153m |J. Phys. Chem. B 2011, 115, 8989–8995

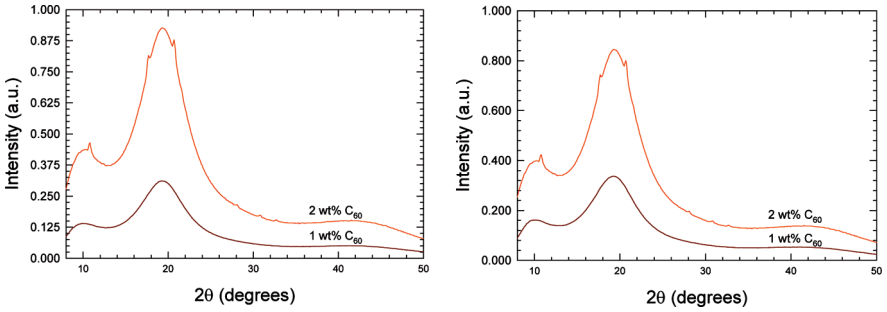

Figure 3. 1D WAXS patterns of (a) PS_6 and (b) PS_{41} with 1 and 2 wt % C_{60}. As indicated by the appearance of crystalline peaks associated with C_{60}, the miscibility limit for both systems is between 1 and 2 wt %.

Table 1. DFT Results for C_{60}−Oligomer Interactions

oligomer structure	binding energy (eV)	electrons donated
PS	0.24	0.16
P2VN	0.31	0.10
P9VPh	0.43	0.12

P2VN and P9VP with the addition of one additional phenyl ring is unexpected. It could be suspected that the low molecular weight the P9VPh in comparison to both the PS and P2VN systems investigated could explain this result. Therefore, additional measurements were made using PS with molecular weights similar to P2VN and P9VPh to determine if this was a factor in the degree of increased miscibility seen with P9VPh.

The results of WAXS measurements with PS (M_n = 6240 g/mol) (PS_6) and PS (M_n = 41,400 g/mol) (PS_{41}) are shown in Figure 3. As indicated by the 1D WAXS patterns of both systems, the miscibility limit of C_{60} is between 1 and 2 wt %. This value is slightly higher than that seen for PS with a M_n of 100 000 g/mol (PS_{100}) and only slightly lower than that of the P2VN−C_{60} system investigated. The marginal increase in miscibility is clearly due to the effects of lower molecular weight in both systems. However, these results also show that molecular weight effects are not responsible for the magnitude of the miscibility increase seen with C_{60}−P9VPh blends.

All-electron quantum density functional theory (DFT) calculations were used to provide additional insight into the extent of molecular interaction between oligomer units and C_{60}. Table 1 shows the DFT calculation results for binding energy and electrons donated for each oligomer−C_{60} system. The results indicate that the binding energy increases with increasing aromaticity, and that the increase is nonlinear. This is entirely consistent with the observed experimentally determined solubility limit, as shown in Figure 4. However, based on the simulation results, this is not due to an increase in electrons donated as there is no consistent change in this from system to system.

Comparing the simulation results of binding energy to the miscibility limits observed experimentally with increasing number of phenyl rings in the vinyl side group, the experimental results agree well with the trend seen in the simulations. Both binding energy and miscibility limit increase with increasing aromaticity as shown in Figure 4. The molecular origin of this increased interaction strength induced by the phenyl group is, however, not clear. Increased $\pi-\pi$ interactions with the C_{60} cage would be expected for these phenyl groups. This would be promoted most strongly if the phenyl groups were oriented

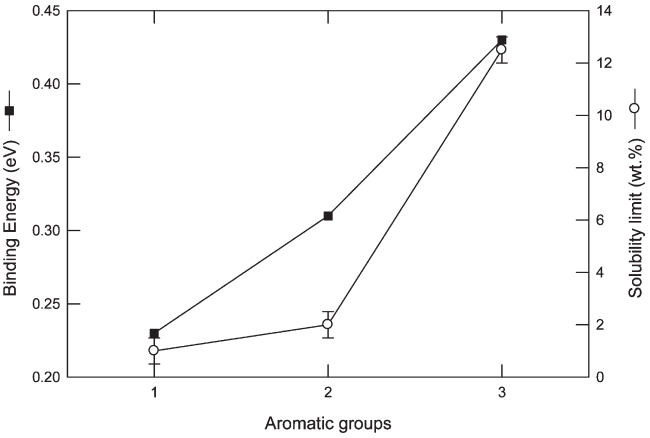

Figure 4. Comparison of miscibility limit of C_{60} with polymers with binding energy calculated for C_{60}−oligomer systems as a function of number of aromatic groups.

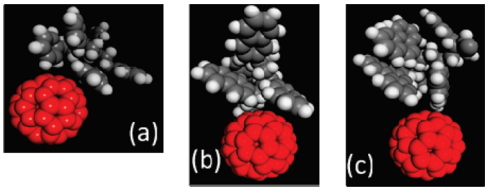

Figure 5. Optimized conformation of oligomer−C_{60} systems of (a) PS, (b) P2VN, and (c) P9VPh.

parallel to the tangent of the C_{60}. Another favorable orientation would be if the phenyl group is perpendicular with the C_{60} tangent, i.e., a T-junction configuration.[55] We have therefore undertaken more detailed analysis of the geometric conformation for the DFT models. As can be seen from the molecular images in Figure 5 in each case the lowest energy conformation has the phenyl groups closest to the C_{60} with the backbone further away. This suggests it is the phenyl groups that are largely responsible for the interaction with the fullerene and not the sp^3 carbons in the backbone. The angle between the plane of each of the phenyl side groups and the tangent of the C_{60} (i.e., φ) as defined in Figure 6 has been calculated and reported in Table 2. As can be seen, there are very few phenyl groups that are either parallel or in a T-orientation with respect to the C_{60}. Neither is there any difference in the number of the two strongest interacting conformational orientations, in the three oligomers as

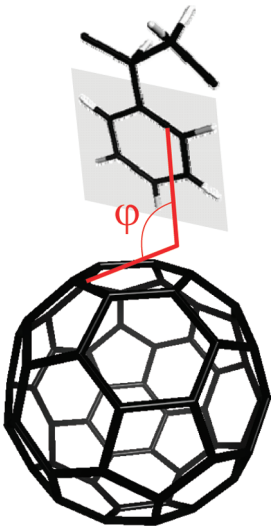

Figure 6. Definition of angle, φ, between plane of phenyl group and tangent of C_{60}.

Table 2. Minimum Distance between C_{60} and Nearest C in the Phenyl Ring (d_{min}) and the Angle between Planes φ (Defined in Figure 6) Determined from DFT Optimized Geometry Calculations

oligomer	phenyl no.	d_{min} (Å)	φ (deg)
PS	1	2.88	42.0
	2	1.79	9.5
	3	3.32	60.6
	4	2.72	70.2
	5	2.08	61.2
P2VP	1	3.38	45.3
	2	2.50	26.0
	3	2.99	68.2
	4	2.11	31.8
	5	1.83	39.6
P9VPh	1	2.33	71.1
	2	2.21	54.6
	3	1.92	3.2
	4	3.06	59.9
	5	2.52	26.7

shown by the average value of φ of 43 ± 27°, 42 ± 16°, and 49 ± 24°, for PS, P2VP, and P9VPh, respectively. This behavior is quite unlike the interactions observed in aromatic small molecule interactions with fullerenes, where molecular reorientation of the small molecules is possible to enable strong $\pi-\pi$ and T-junction interactions with the fullerene. In the polymers, these orientations are not possible due to the connectivity with the backbone, which significantly restricts conformations the phenyl groups can take relative to the fullerene.

Further analysis of the DFT structures show that the minimum distance of the closest C-atom of the phenyl groups and the fullerene (d_{min}) for the three different polymers within the statistics are the same, with average values of d_{min} = 2.6 ± 0.6 Å, 2.6 ± 0.6 Å, and 2.4 ± 0.4 Å, for PS, P2VP, and P9VPh, respectively. These DFT results were compared to the results from wide-angle neutron scattering (WANS) measurements of

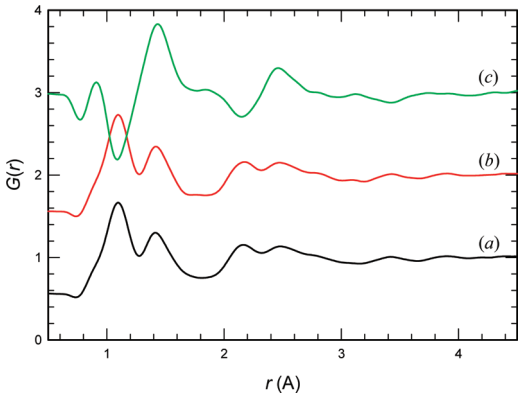

Figure 7. Radial distribution function curves obtained from wide angle neutron scattering measurements for dPS (a), dPS + 2 wt % C_{60} (b), and hPS + 2 wt % C_{60} (c).

dPS, dPS+ 2 wt % C_{60}, and hPS + 2 wt % C_{60}. In these samples the weight fraction of fullerenes was chosen to maximize its contribution to the scattering, but at the same time also minimize the effects of aggregation. The use of hydrogenous and deuterated samples allows determination whether the $G(r)$ peaks are associated with C−H or C−C distances, because C−H and C−D peaks will have opposite phases. The radial distribution function for dPS+ 2 wt % C_{60} is of course dominated by the presence of the PS and therefore shows significant similarity with the pure PS data (see Figure 7). The hPS+ 2 wt % C_{60} data although clearly different shows some commonality to its deuterated analogue associated with peak phase changes for peaks associated distances involving. To compare directly with the data from the DFT, the $G(r)$ data were analyzed in the region of r between 1.8 and 3 Å using Gaussian peak fitting analysis. As shown in Figure 8a for dPS, the data could be fitted with three peaks at r = 2.14 ± 0.14 Å, 2.47 ± 0.21 Å, and 2.79 ± 0.15 Å (R^2 = 0.999). Comparison with the hPS + 2 wt % C_{60} data indicates the peak at 2.14 Å is associated with distances involving H/D.

The other two peaks in this limited distance regime are also observed in the hydrogenated sample and are therefore associated with C−C distances. The best fits to the dPS + 2 wt % C_{60} radial distribution data were obtained using four peaks at r = 2.15 ± 0.14 Å, 2.47 ± 0.19 Å, 2.66 ± 0.10 Å, and 2.81 ± 0.11 Å (R^2 = 0.998) (see Figure 8b). The additional peak (compared to pure dPS) at 2.66 Å is a C−C dimension that within experimental error is entirely consistent with the C−C distances for the phenyl−fullerene distances determined from the DFT calculations. Despite the size limitations for the DFT-D calculations, the results are completely consistent with the experimental results, giving very strong confidence of the validity of the computational approach.

Because the polymer−fullerene interactions are nonspecific, i.e., van der Waals, the strength of the interaction therefore relies on the number of interactions rather than strong $\pi-\pi$ interactions that are seen in solvents such as the naphthalenes, calixarenes, or corannulene.[56] Given that the interaction geometries for these three polymers are the same, it suggests that the increase binding energy is due to the increase of bonding interactions associated with the increase in sp^2 carbons between PS and P9VPh. The step increase between P2VN and P9VPh, we believe, is due to the configuration of the three phenyl groups in the vinyl phenanthrene, which is approximately conformal with the curvature of the C_{60}.

dx.doi.org/10.1021/jp203153m |J. Phys. Chem. B 2011, 115, 8989–8995

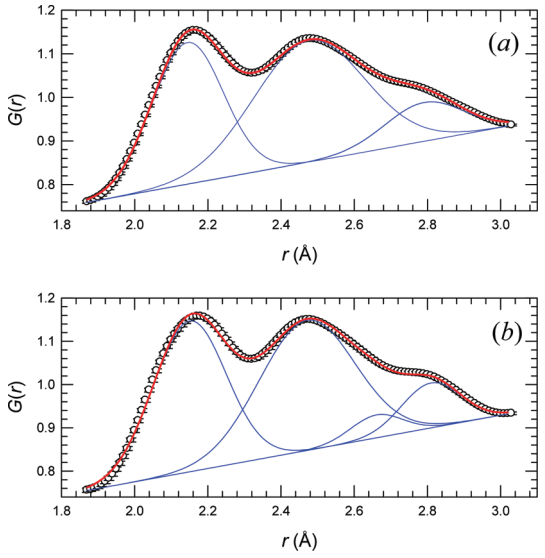

Figure 8. Radial distribution functions data for (a) dPS and (b) dPS + 2 wt % C_{60}. The experimental data are the filled points, with fits to the data shown as the solid red line. The contributing Gaussian peaks are shown in blue.

These orientations are very different from that for a similar diameter carbon nanotube, which would have the same local curvature but, due to the availability of a 1D periodic axis along the nanotube, could support face-down orientations.[57] We also mention that, in general, the interaction energies between spatially small monomers and C_{60} tend to be larger than those for single-walled carbon nanotubes when the orientation of the monomers are the same in part due to the presence of pentagons in the sp^2 network of C_{60}.

CONCLUSIONS

Using wide-angle X-ray scattering, we have shown that solubility of fullerene C_{60} increases with increasing aromaticity in a homologous series of vinyl polymers. The solubility increase is, however, nonlinear with number of aromatic side groups in the polymer from ~1 wt % for PS to 12 wt % in P9VPh. DFT results were found to correlate well with our experimental data and also show a nonlinear increase in binding energy between oligomers of C_{60}. Analysis of the energetically favored conformations show that all the intermolecular interactions result from the oligomeric phenyl side groups with the C_{60} cage. The extent of these intermolecular interactions are mediated by the polymeric backbone, which although it does not play a direct role in the intermolecular interactions it does hinder the ability of the phenyl side groups to arrange themselves into planar $\pi-\pi$ stacking or T-junction conformations. The DFT calculations show that the increase in binding energy (observed experimentally as an increase in solubility limit) is due to the increasing number of molecular interactions between the phenyl moieties and the C_{60}. The nonlinearity of this increase is believed to be due to the slight curvature associated with the configuration of phenyl groups in the phenanthrene side groups.

AUTHOR INFORMATION

Corresponding Author

*E-mail: bucknall@gatech.edu.

ACKNOWLEDGMENT

This work was partially funded by the NSF under the Materials World Network program (DMR-0710467). B.G.S. was supported by the Center for Nanophase Materials Sciences, which is sponsored at Oak Ridge National Laboratory by the Office of Basic Energy Sciences, U.S. Department of Energy. ISIS Facility, Rutherford Appleton Lab, U.K., are acknowledged for beamtime on the SANDALS WANS instrument. Prof. A. Soper and Dr. S. Imberti are thanked for their assistance in WANS measurements.

REFERENCES

(1) Hansen, C. M.; Smith, A. L. *Carbon* **2004**, *42*, 1591.
(2) Heymann, D. *Carbon* **1996**, *34*, 627.
(3) Huang, J.-C. *Fluid Phase Equilib.* **2005**, *237*, 186.
(4) Kadish, K. M., Ruoff, R. S. *Fullerenes: chemistry, physics, and technology*; Wiley-IEEE: New York, 2000.
(5) Ruoff, R. S.; Tse, D. S.; Malhotra, R.; Lorents, D. C. *J. Phys. Chem.* **1993**, *97*, 3379.
(6) Ruoff, R. S.; Malhotra, R.; Huestis, D. L.; Tse, D. S.; Lorents, D. C. *Nature* **1993**, *362*, 140.
(7) Sivaraman, N.; Dhamodaran, R.; Kaliappan, I.; Srinivasan, T. G.; Rao, P. R. V.; Mathews, C. K. *J. Org. Chem.* **1992**, *57*, 6077.
(8) Sivaraman, N.; Srinivasan, T. G.; Rao, P. R. V. *J. Chem. Inf. Comput. Sci.* **2001**, *41*, 1067.
(9) Smith, A. L.; Walter, E.; Korobov, M. V.; Gurvich, O. L. *J. Phys. Chem.* **1996**, *100*, 6775.
(10) Tomiyama, T.; Uchiyama, S.; Shinohara, H. *Chem. Phys. Lett.* **1997**, *264*, 143.
(11) Toropov, A. A.; Bakhtiyor, F. R.; Leszczynska, D.; Leszczynski, J. *Chem. Phys. Lett.* **2007**, *444*, 209.
(12) Toropov, A. A.; Leszczynska, D.; Leszczynski, J. *Chem. Phys. Lett.* **2007**, *441*, 119.
(13) Ahn, J. S.; Suzuki, K.; Iwasa, Y.; Mitani, T. *J. Lumin.* **1997**, *72*–*74*, 464.
(14) Alfe, M.; Apicella, B.; Barbella, R.; Bruno, A.; Ciajolo, A. *Chem. Phys. Lett.* **2005**, *405*, 193.
(15) Alfe, M.; Barbella, R.; Bruno, A.; Minutolo, P.; Ciajolo, A. *Carbon* **2005**, *43*, 651.
(16) Baltog, I.; Baibarac, M.; Mihut, L.; Preda, N.; Velula, T.; Lefrant, S. *Rom. Rep. Phys.* **2005**, *57*, 837.
(17) Bensasson, R. V.; Bienvenue, E.; Dellinger, M.; Leach, S.; Seta, P. *J. Phys. Chem.* **1994**, *98*, 3492.
(18) Bezmelnitsin, V. N.; Eletskii, A. V.; Stepanov, E. V. *J. Phys. Chem.* **1994**, *98*, 6665.
(19) Bulavin, L. A.; Adamenko, I. I.; Yashchuk, V. M.; Ogul'chansky, T. Y.; Prylutskyy, Y. I.; Durov, S. S.; Scharff, P. *J. Mol. Liq.* **2001**, *93*, 187.
(20) Nath, S.; Pal, H.; Palit, D. K.; Sapre, A. V.; Mittal, J. P. *J. Phys. Chem. B* **1998**, *102*, 10158.
(21) Nath, S.; Pal, H.; Sapre, A. V. *Chem. Phys. Lett.* **2000**, *327*, 143.
(22) Nath, S.; Pal, H.; Sapre, A. V. *Chem. Phys. Lett.* **2002**, *360*, 422.
(23) Rudalevige, T.; Francis, A. H.; Zand, R. *J. Phys. Chem. A* **1998**, *102*, 9797.
(24) Torok, G.; Lebedev, V. T.; Cser, L. *Phys. Solid State* **2002**, *44*, 572.
(25) Yevlampieva, N. P.; Biryulin, Y. F.; Melenevskaja, E. Y.; Zgonnik, V. N.; Rjumtsev, E. I. *Colloids Surf., A* **2002**, *209*, 167.
(26) Ying, Q.; Marecek, J.; Chu, B. *J. Chem. Phys.* **1994**, *101*, 2665.
(27) Qiao, J. L.; Gong, Q. J.; Du, L. M.; Jin, W. J. *Spectrochim. Acta Part A* **2001**, *57*, 17.
(28) Scurlock, R. D.; Ogilby, P. R. *J. Photochem. Photobiol., A* **1995**, *91*, 21.
(29) Seshadri, R.; D'Souza, F.; Krishnan, V.; Rao, C. N. R. *Chem. Lett.* **1993**, 217.
(30) Sibley, S. P.; Campbell, R. L.; Silber, H. B. *J. Phys. Chem.* **1995**, *99*, 5274.

(31) Sibley, S. P.; Nguyen, Y. T.; Campbell, R. L.; Silber., H. B. *Spectrochim. Acta Part A* **1997**, *53*, 679.
(32) Wang, Y. *J. Phys. Chem.* **1992**, *96*, 764.
(33) Laiho, A.; Ras, R. H. A.; Valkama, S.; Ruokolainen, J.; Sterbacka, R.; Ikkala, O. *Macromolecules* **2006**, *39*, 7648.
(34) Chen, J.; Liu, H.; Weimer, W. A.; Halls, M. D.; Waldeck, D. H.; Walker, G. C. *J. Am. Chem. Soc.* **2002**, *124*, 9034.
(35) Moore, V. C.; Strano, M. S.; Haroz, E. H.; Hauge, R. H.; Smalley, R. E. *Nano Lett.* **2003**, *3*, 1379.
(36) Nish, A.; Hwang, J.-Y.; Doig, J.; Nicholas, R. J. *Nat. Nanotechnol.* **2007**, *2*, 640.
(37) Murakami, H.; Nomura, T.; Nakashima, N. *Chem. Phys. Lett.* **2003**, *378*, 481.
(38) O'Connell, M. J.; Boul, P.; Ericson, L. M.; Huffman, C.; Wang, Y.; Haroz, E.; Kuper, C.; Tour, J.; Ausman, K. D.; Smalley, R. E. *Chem. Phys. Lett.* **2001**, *342*, 265.
(39) Gutierrez-Nava, M.; Nierengarten, H.; Masson, P.; Van Dorsselaer, A.; Nierengarten, J.-F. *Tetrahedron Lett.* **2003**, *44*, 3043.
(40) Sapurina, I.; Mokeev, M.; Lavrentev, V.; Zgonnik, V.; Trchova, M.; Hlavata, D.; Stejskail, J. *Eur. Polym. J.* **2000**, *36*, 2321.
(41) Yamaguchi, Y.; Kobayashi, S.; Amita, N.; Wakamiya, T.; Matsubara, Y.; Sugimoto, K.; Yoshida, Z. *Tetrahedron Lett.* **2002**, *43*, 3277.
(42) Benesi, H. A.; Hildebrand, J. H. *J. Am. Chem. Soc.* **1949**, *71*, 2703.
(43) Waller, J. H.; Bucknall, D. G.; Register, R. A.; Beckham, H. W.; Leisen, J.; Campbell, K. *Polymer* **2009**, *50*, 4199.
(44) Mathis, C. S., B.; Brinkmann, M. *Compt. Rend. Chim.* **2006**, 1075.
(45) Okamura, H.; Minoda, M.; Fukuda, T.; Miyamoto, T.; Komatsu, K. *Macromol. Rapid Commun.* **1999**, *20*, 37.
(46) Schmaltz, B.; Brinkmann, M.; Mathis, C. *Macromolecules* **2004**, *37*, 9056.
(47) Kendall, R. A.; Apra, E.; Bernholdt, D. E.; Bylaska, E. J.; Dupuis, M.; Fann, G. I.; Harrison, R. J.; Ju, J. L.; Nichols, J. A.; Nieplocha, J.; Straatsma, T. P.; Windus, T. L.; Wong, A. T. *Comput. Phys. Commun.* **2000**, *129*, 260.
(48) Hehre, W. J.; Ditchfie, R.; Pople, J. A. *J. Chem. Phys.* **1972**, *56*, 2257.
(49) Vazquez-Mayagoitia, A.; Sherrill, C. D.; Apra, E.; Sumpter, B. G. *J. Chem. Theory Comput.* **2010**, *6*, 727.
(50) Sherrill, C. D.; Sumpter, B. G.; Sinnokrot, M. O.; Marshall, M. S.; Hohenstein, E. G.; Walker, R. C.; Gould, I. R. *J. Comput. Chem.* **2009**, *30*, 2187.
(51) Burns, L. A.; Vazquez-Mayagoitia, A.; Sumpter, B. G.; Sherrill, C. D. *J. Chem. Phys.* **2011**, *134*, 084107.
(52) Sumpter, B. G.; Jiang, D. E.; Meunier, V. *Small* **2008**, *4*, 2035.
(53) Meunier, V.; Sumpter, B. G. *J. Chem. Phys.* **2005**, *123*, 8.
(54) Sumpter, B. G.; Meunier, V.; Valeev, E. F.; Lampkins, A. J.; Li, H.; Castellano, R. K. *J. Phys. Chem. C* **2007**, *111*, 18912.
(55) Ringer, A. L.; Sinnokrot, M. O.; Lively, R. P.; Sherrill, C. D. *Chem.—Eur. J.* **2006**, *12*, 3821.
(56) Sygula, A.; Fronczek, F. R.; Sygula, R.; Rabideau, P. W.; Olmstead, M. M. *J. Am. Chem. Soc.* **2007**, *129*, 3842.
(57) Linton, D.; Driva, P.; Sumpter, B.; Ivanov, I.; Geohegan, D.; Feigerle, C.; Dadmun, M. D. *Soft Matter* **2010**, *6*, 2801.